Transport Properties of Ar-Kr Mixtures: A Molecular Dynamics Simulation Study

Sun Hong Min, Chang Mo Son, and Song Hi Lee*

*Department of Chemistry, Kyungsung University, Busan 608-736, Korea. *E-mail: shlee@ks.ac.kr*
Received July 2, 2007

Equilibrium molecular dynamics (EMD) simulations are used to evaluate the transport coefficients of argon-krypton mixtures at two liquid states (state A: 94.4 K and 1 atm; state B: 135 K and 39.5 atm) *via* modified Green-Kubo formulas. The composition dependency of the volume at state A obeys close to the linear model for ideal liquid mixture, while that at state B differs from the linear model probably due to the high pressure. The radial distribution functions for the Ar-Kr mixture (x = 2/3) show a mixing effect: the first peak of g_{11} is higher than that of g(r) for pure Ar and the first peak of g_{22} is lower than that of g(r) for pure Kr. An exponential model of engineering correlation for diffusion coefficient (D) and shear viscosity (η) is superior to the simple linear model for ideal liquid mixtures. All three components of thermal conductivity ($\lambda_{\rho m}$, λ_{tm}, and λ_{ti}) at state A and hence the total thermal conductivity decrease with the increase of x. At state B, the change in λ_{tm} is dominant over those in $\lambda_{\rho m}$ and λ_{ti}, and hence the total thermal conductivity decrease with the increase of x.

Key Words : Diffusion, Shear viscosity, Thermal conductivity, Ar-Kr mixtures, Molecular dynamics simulation

Introduction

The first computer simulation study for the equation of state of an equimolar binary mixture of nearly equal hard spheres was carried out by Rotenberg in the 1960s using Monte Carlo method.[1] An extensive series of computations for Lennard-Jones mixtures followed in the 1970s to determine the excess thermodynamic functions of mixing.[2,3] After that, a number of molecular dynamics studies on the transport coefficients in binary fluid mixtures have been reported.[4-6] There was good agreement among these studies, and therefore it can be said that the basic method to calculate the transport coefficients by MD simulations has been established.

Transport coefficients - self-diffusion coefficient, D, shear viscosity, η, and thermal conductivity, λ- of pure fluids can be calculated from equilibrium molecular dynamics simulation by the infinite time integral of an equilibrium correlation function of the form known as the Green-Kubo formulas.[7-9] Associated with any expression of the Green-Kubo formulas there is also the Einstein formula to calculate the transport properties. In recent years, non-equilibrium molecular dynamics (NEMD) simulations have emerged as a powerful tool for the study of transport coefficients of both simple and molecular fluids.[10-12]

There has only been slow progress in simulating the transport coefficients of fluid mixtures. This in part due to uncertainty concerning the statistical mechanical expressions for the transport coefficients.[13-15] Mixtures have the transport coefficients of D, η, and λ as for a single component fluid.[15-23] There are also additional transport coefficients that have no counterpart in the single component fluids. These include the cross transport coefficients, D^T, thermal diffusion (the Soret effect) and the diffusion thermo-effect (the Dufour effect) which are numerically identical in the linear response regime according to the Onsager reciprocal relation. Molecular dynamics simulation has been used to calculate these.[13-17]

Simulation has also been used to determine the effects of mass and well-depth ratios on the thermal conductivity and shear viscosity of model binary mixtures. Evans and Hanley computed the shear viscosity of binary SS mixtures for several size and mass ratios.[24,25] They proposed a conformal-solution theory of shear viscosity, which was very successful for combined mass and well-depth ratios up to ~5. This treatment has been extended with similar success to thermal conductivity and again for shear viscosity.[26]

In the present paper, we perform equilibrium molecular dynamics (EMD) simulations of pure argon, pure krypton, and their mixtures. The goal of this paper is to elucidate the dependence of transport properties of Ar-Kr mixtures on mole fraction of krypton, x.

This paper is organized as follows: We present the molecular models and details of MD simulation methods in next section, theories for dynamic properties in Section III, our simulation results in Section IV, and concluding remarks in Section V.

Molecular Models and NpT MD Simulation Methods

We begin by considering a mixture of argon and krypton at two states of constant temperatures and pressures - state A: 94.4 K and 1 atm, and state B: 135 K and 39.5 atm. For the study of mixture properties, the Lennard-Jones (LJ) potential is used for the Ar-Ar, Ar-Kr, Kr-Kr potentials. The LJ potential parameters for these potentials are given in Table 1 and are derived on the basis of liquid state thermodynamic properties.[2,3,27] The potential curves are depicted in Figure 1. The cross interaction parameters between Ar and Kr are calculated from the simple Lorentz-Berthelot rules:

Table 1. Lennard-Jone parameters for Ar/Ar, Kr/Kr, and Ar/Kr interactions

Interaction	σ(nm)	ε/k_B(K)
Ar-Ar	0.3405	119.8
Kr-Kr	0.3633	167.0
Ar-Kr	0.3519	141.4

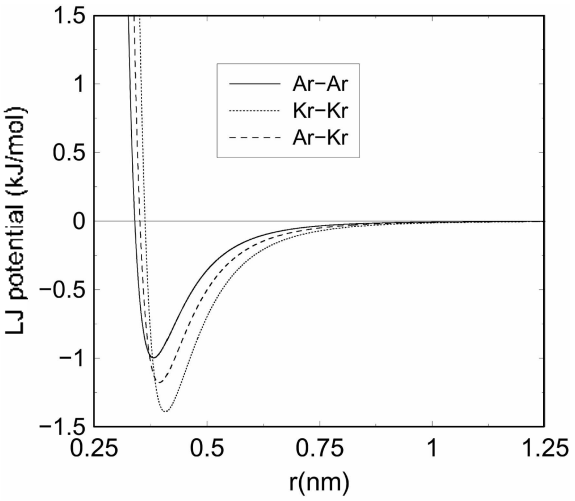

Figure 1. Lennard-Jones potentials for Ar-Ar, Kr-Kr, and Ar-Kr as a function of inter-particle distance.

$$\varepsilon_{ij} = (\varepsilon_i \varepsilon_j)^{1/2} \text{ and } \sigma_{ij} = \frac{\sigma_i + \sigma_j}{2} \tag{1}$$

The use of the LJ potential is motivated by the extensive existing published results on the transport properties of the LJ fluid, as well as the ease with which it can be extended to more complex systems by the addition of dipolar and quadrupolar interactions.

The equations of motion in NpT ensemble are given by

$$d\boldsymbol{r}_i/dt = \boldsymbol{p}_i/m_i + \kappa \boldsymbol{r}_i \tag{2a}$$

$$d\boldsymbol{r}_i/dt = \boldsymbol{F}_i - \dot{\kappa}\boldsymbol{r}_i - \alpha \boldsymbol{p}_i \tag{2b}$$

and

$$dV/dt = 3\dot{\kappa}V, \tag{2c}$$

where $\boldsymbol{r}_i$, m_i, and $\boldsymbol{p}_i$ are the position, mass, and momentum, respectively, of molecule i, $\boldsymbol{F}_i$ is the force exerted by the other molecules on molecule i, and a is the thermosttating constant, given by

$$\alpha = \frac{\sum_i^N \boldsymbol{p}_i \cdot \boldsymbol{F}_i}{\sum_i^N \boldsymbol{p}_i^2} - \dot{\kappa}. \tag{3}$$

The effect of the thermosttating term involving $\alpha \boldsymbol{p}_i$ in Eq. (2b) is to hold the translational kinetic energy constant. The functional form of this term is derived by Gauss's principle of least constraint.[28] The momenta in Eqs. (2a) and (2b) are measured with respect to the streaming velocity of the fluid and are known as peculiar momenta. In similar fashion to the thermosttating constant, the dilation rate $\dot{\kappa} = d\kappa/dt$ controls the volume of the system in order to constrain the pressure p. The pressure is one third of the trace of the pressure tensor $\boldsymbol{P}$, which is expressed in terms of molecular quantities by

$$P = \frac{1}{V}\left[\sum_{i=1}^{N} m_i \boldsymbol{v}_i \boldsymbol{v}_i + \sum_{i<j}^{N} \boldsymbol{r}_{ij}\boldsymbol{f}_{ij}\right], \tag{4}$$

where V is the volume of the system, $\boldsymbol{r}_{ij}=\boldsymbol{r}_i-\boldsymbol{r}_j$ is the vector joining the centers of molecular i and j, and $\boldsymbol{F}_{ij}$ is the force between them. The equation of motion for the dilation rate for a pure fluid is given by Hood *et al.*[29] The extension to mixtures is straightforward and the dilation rate is given by

$$\dot{\kappa} = -\frac{\sum_{i<j}^{N} (\boldsymbol{r}_{ij} \cdot \boldsymbol{p}_{ij})(\Phi_{ij}'' + \Phi_{ij}'/r_{ij})}{m\sum_{i<j}^{N} r_{ij}^2(\Phi_{kj}'' + \Phi_{ij}'/r_{ij}) + 9pV}, \tag{5}$$

where Φ_{ij} is the interaction potentials between molecular i and j. Putting $\dot{\kappa}$=0 in Eqs. (2) recovers the NVT ensemble.

The preliminary canonical ensemble (NVT fixed) EMD simulation of 1728 argon atoms was started in the cubic box of length L=4.3696 nm, of which the density is equal to 1.374 g/cm^3 at 94.4 K and 1 atm. The inter-atomic potential was truncated at 2.25 σ_{Kr}, which is the cutoff distance used in many other simulations. Long range corrections to the energy, pressure, *etc.* due to the potential truncation were included in these properties by assuming that the pair distribution function was uniform beyond the cutoff distance.[30] Initially the equations of motion were solved using the velocity Verlet algorithm[31] with a time step of 10^{-14} second, but later it was switched to a fifth-order predictor-corrector Gear integration[32] for NpT EMD simulation. The systems were fully equilibrated and the equilibrium properties were averaged over five blocks of 100,000 time steps (1 nanosecond). The brief summary of thermodynamic averages for pure Ar and Kr liquids at two states are given in Tables 2 and 3. The configurations of argon atoms were stored every time step for further analysis.

Green-Kubo Formula

As dynamic properties, we consider diffusion constant (D), shear viscosity (η), and thermal conductivity (λ) of Ar-Kr mixture systems. Diffusion constant can be obtained through two routes: the Green-Kubo formula from velocity auto-correlation functions (VAC):

$$D_s = \frac{1}{3}\int_0^{\infty} < \boldsymbol{v}_i(t) \cdot \boldsymbol{v}_i(0) > dt. \tag{6a}$$

and the Einstein formula from mean square displacements (MSD):

$$D_s = \frac{1}{6}\lim_{t\to\infty} \frac{d<|\boldsymbol{r}(t) - \boldsymbol{r}(0)|^2}{dt}. \tag{6b}$$

Shear viscosity is calculated by the modified Green-Kubo

formula for better statistical accuracy[33]:

$$\eta = \frac{V}{kT}\int_0^\infty dt \sum_i \langle P_{i\alpha\beta}(0)\cdot P_{i\alpha\beta}(t)\rangle , \quad (7)$$

where $P_{i\alpha\beta}(t) = \frac{1}{V}[mv_{i\alpha}(t)\cdot v_{i\beta}(t) - \sum_{j\neq i} r_{i\alpha}(t)\cdot f_{i\beta}(t)]$

with $a\beta$= xy, xz, yx, yz, zx, and zy.

Thermal conductivity is also calculated by the modified Green-Kubo formula for better statistical accuracy[33]:

$$\lambda = \frac{V}{kT^2}\int_0^\infty dt \sum_i \langle \dot{q}_{i\alpha}(0)\cdot \dot{q}_{i\alpha}(t)\rangle , \quad (8)$$

where a = x, y, and z. The heat flux by each molecule is

$$\dot{q}_{i\alpha}(t) = \frac{1}{V}\left\{ \varepsilon_i(t)\cdot v_{i\alpha}(t) + \frac{1}{2}\sum_{j\neq i} r_{ij\alpha}(t)\cdot [v_i(t)\cdot f_{ij}(t)] \right\}. \quad (9)$$

Here, the energy of molecule i is given by

$$\varepsilon_i(t) = \frac{1}{2}m_i v_i(t)^2 - \frac{1}{2}\sum_{j\neq i}\Phi[r_{ij}(t)] . \quad (10)$$

The heat flux by each molecule, Eq. (9), with the energy of molecule, Eq. (10), consists of three contributions:

$$\dot{q}_{i\alpha} = \dot{q}_{i\alpha}^{tm} + \dot{q}_{i\alpha}^{pm} - \dot{q}_{i\alpha}^{ti} , \quad (11)$$

where

$$\dot{q}_{i\alpha}^{tm} = \frac{1}{V}\left[\frac{1}{2}m_i v_i^2\right] v_{i\alpha} , \quad (12)$$

$$\dot{q}_{i\alpha}^{pm} = \frac{1}{V}\left[\frac{1}{2}\sum_{j\neq i}\Phi(r_{ij})\right] v_{i\alpha} , \quad (13)$$

and

$$\dot{q}_{i\alpha}^{ti} = \frac{1}{V}\left[\frac{1}{2}\sum_{j\neq i} r_{ij\alpha}(v_i\cdot f_{ij})\right], \quad (14)$$

$\dot{q}_{i\alpha}^{tm}$ and $\dot{q}_{i\alpha}^{pm}$ are the translational and the potential energy transport, respectively, due to molecular motion and $\dot{q}_{i\alpha}^{ti}$ is the translational energy transfer due to molecular interaction. Hence, the thermal conductivity, Eq. (8), consists of three contributions:

$$\lambda_{tot} = \lambda_{tm} + \lambda_{pm} + \lambda_{ti} . \quad (15)$$

Results and Discussion

We begin by reporting thermodynamic properties for pure liquids using the LJ potentials in NpT ensembles. The thermodynamic properties at two states [(A) T = 94.4 K and p = 1 atm; (B) T = 135 K and p = 39.5 atm] are summarized in Table 2 for pure Ar and in Table 3 for pure Kr. For both Ar and Kr, it is clear that the EMD simulation results predict the density and energy very accurately [within 1.1% (state A) and 4.4% (state B) of the Ar density and 0.7% (state B) of the Kr density, and within 0.1% (state B) of the Ar energy and 2.2% of the Kr energy]. The pressures for state A are negative and are less accurately predicted. However, pressure as measured in molecular simulations exhibits considerable sensitivity to the details of the cutoff procedure, so that the error in the pressure for state A can be regarded as quite small.

Volume, LJ and total energies, increasing in steps of 1/6 in the Kr mole fraction x, are given in Table 2 for state A (T = 94.4 K and p = 1 atm) and in Table 3 for state B (T = 135 K and p = 39.5 atm). Note that the volume for pure Kr is less than that for pure Ar at state B probably due to the high pressure (39.5 atm). The experimental volumes for pure liquids give the same trend (110.8 nm^3 for pure Ar and 103.9 nm^3 for pure Kr). The composition dependencies of the volume and energies are also shown in Figures 2 and 3. For ideal liquid mixtures, one would expect that each of the properties would depend linearly on composition, *i.e.*,

$$Y = (1-x)Y_{Ar} + xY_{Kr} , \quad (16)$$

where Y is a property. The linear model for each property is shown in the figures as a solid line. Clearly, the volume at

Table 2. Pure argon system at two states [(A) T = 94.4 K and p = 1 atm; (B) T = 135 K and p = 39.5 atm] in NpT ensembles. LJ energy (E_{LJ} in kJ/mol), total energy (E_{tot} in kJ/mol), density (ρ in g/cm^3) and pressure (p in atm). Uncertainties in the last reported digit(s) are given in parenthesis

States	A (94.4 K and 1 atm)				B (135 K and 39.5 atm)			
Property	p	ρ	$-E_{LJ}$	$-E_{tot}$	p	ρ	$-E_{LJ}$	$-E_{tot}$
Expt.	1	1.374	–	–	39.5	1.034	–	2.432
Npt EMD	−0.542(4)	1.359(16)	5.400(5)	4.222(5)	39.02(1)	1.079(21)	4.118(7)	2.434(7)

Table 3. Pure krypton system at two states [(A) T = 94.4 K and p = 1 atm; (B) T = 135 K and p = 39.5 atm] in NpT ensembles. LJ energy (E_{LJ} in kJ/mol), total energy (E_{tot} in kJ/mol), density (ρ in g/cm^3) and pressure (p in atm). Uncertainties in the last reported digit(s) are given in parenthesis

States	A (94.4 K and 1 atm)				B (135 K and 39.5 atm)			
Property	p	ρ	$-E_{LJ}$	$-E_{tot}$	p	ρ	$-E_{LJ}$	$-E_{tot}$
Expt.	1	–	–	–	39.5	2.315	–	5.563
Npt EMD	−1.734(3)	2.607(18)	8.517(4)	7.339(4)	37.83(5)	2.331(20)	7.371(9)	5.687(9)

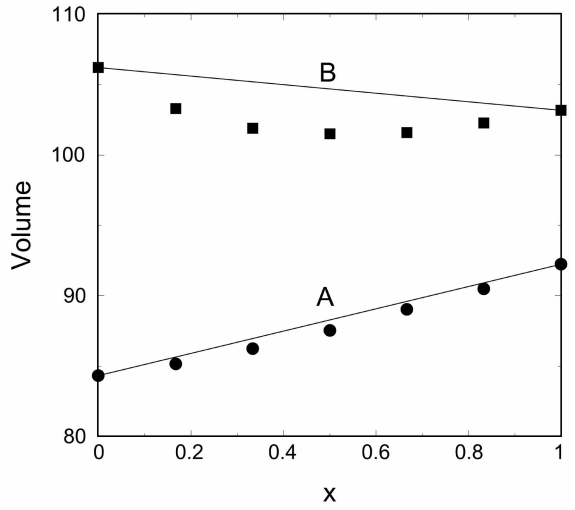

Figure 2. Volume (nm^3) as a function of krypton mole fraction, x, at state A (94.4 K and 1 atm) and at state B (135 K and 39.5 atm) in NpT ensemble. ●: volume of state A, ■: volume of state B.

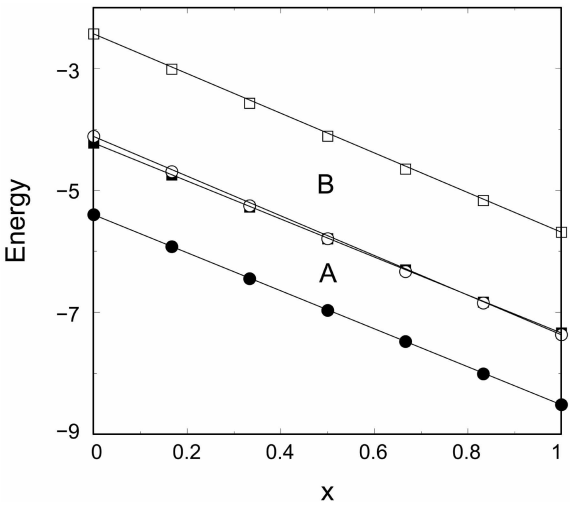

Figure 3. LJ and total energies (E_{LJ} and E_{tot} in kJ/mol) as a function of krypton mole fraction, x, at state A (94.4 K and 1 atm) and at state B (135 K and 39.5 atm) in NpT ensemble. ●: LJ energy of state A, ■: total energy of state A, ○: LJ energy of state B, and □: total energy of state B.

state A is close to the linear model, while that at state B differs noticeably from the linear model. On the other hand, the energies at both states show a perfect linear model.

Figures 4 and 5 show the radial distribution functions for pure liquids and the Ar-Kr mixture (x = 2/3) in NpT ensembles. The radial distribution function, $g(r)$, is defined as

$$g(r) = \frac{1}{\rho_0}\left\langle \frac{Nr,\Delta r}{Vr,\Delta r} \right\rangle \tag{17}$$

where ρ_0 is the bulk density, $N(r,\Delta r)$ is the number of molecules in a shell which is between $r - \Delta r/2$ and $r + \Delta r/2$ from the center of a molecule with $\Delta r = 0.002$ nm, $V(r,\Delta r)$ is the volume of the shell, and $\langle \cdots \rangle$ indicates the corresponding ensemble average. In the radial distribution functions for

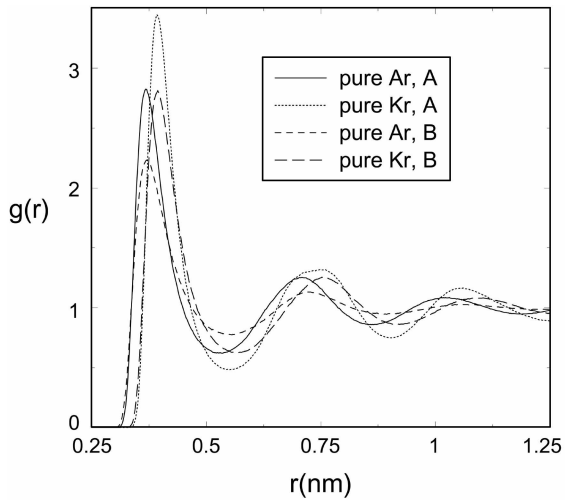

Figure 4. Radial distribution functions of pure argon and pure krypton systems at state A (94.4 K and 1 atm) and at state B (135 K and 39.5 atm) in NpT ensemble.

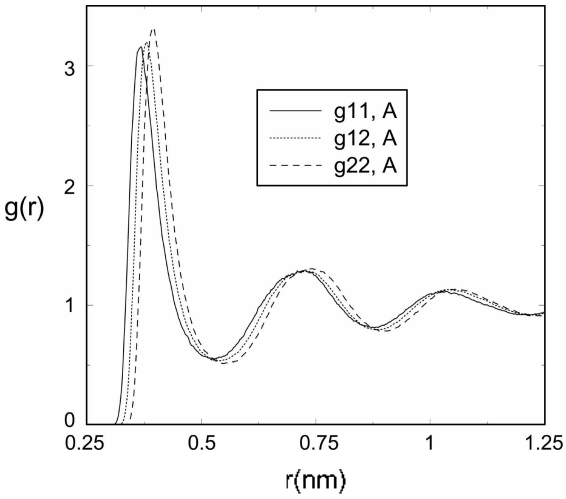

Figure 5. Radial distribution functions of an Ar-Kr mixture system (x = 2/3) at state A (94.4 K and 1 atm) in NpT ensemble.

pure liquids at both states as shown in Figure 4, the positions and the heights of the first peaks reflect the magnitude of the LJ parameters σ and ε, respectively. That is, the smaller σ is, the closer molecules come, and the larger ε is, the more molecules come. Switching from state A to state B causes to decrease the heights of the first peaks keeping the positions of the first peaks same. This implies that the temperature effect dominates over the pressure effect.

Figure 5 shows the radial distribution functions for the Ar-Kr mixture (x = 2/3) at state A. The first peak of g_{11} is higher than that of g(r) for pure Ar and the first peak of g_{22} is lower than that of g(r) for pure Kr. The is a mixing effect. The height of the first peak of g_{12} is between those of g_{11} and g_{22}. Switching from state A to state B for the Ar-Kr mixture (x = 2/3) lowers only the heights of the radial distribution functions (data not shown).

Diffusion constants and viscosities for pure liquids and Ar-Kr mixtures through the Green-Kubo formulas (Eqs. 6(a)

Table 4. Volume (V in nm^3), LJ and total energies (E_{LJ} and E_{tot} in kJ/mol), diffusion constant (D in 10^{-5} cm^2/sec, Eq. (6a)), shear viscosity (η in mp), and thermal conductivities (λ in 10^{-4} cal/Kemsec) of mixtures of argon and krypton at state A (T = 94.4 K and p = 1 atm) as a function of krypton mole fraction, x. Uncertainties in the last reported digit(s) are given in parenthesis

x	V	$-E_{LJ}$	$-E_{tot}$	D	η	λ_{dm}	λ_{pm}	λ_{tr}	λ_{tot}
0	84.32(7)	5.400(5)	4.222(5)	2.560(87)	3.097(31)	0.1466(40)	0.8079(31)	0.7915(65)	1.746(14)
1/6	85.15(4)	5.924(7)	4.747(7)	2.003(49)	4.004(56)	0.1174(18)	0.7535(20)	0.7498(78)	1.621(12)
1/3	86.23(8)	6.449(6)	5.272(6)	1.616(42)	5.122(36)	0.0953(21)	0.7067(19)	0.7247(92)	1.527(13)
1/2	87.52(6)	6.969(6)	5.792(6)	1.249(27)	6.507(27)	0.0765(14)	0.6292(23)	0.7016(66)	1.407(10)
2/3	89.02(5)	7.483(6)	6.305(6)	1.032(27)	8.048(66)	0.0638(15)	0.5883(16)	0.6925(89)	1.345(12)
5/6	90.49(5)	8.010(7)	6.833(7)	0.779(45)	9.916(86)	0.0508(22)	0.5036(29)	0.6814(67)	1.236(12)
1	92.24(6)	8.517(4)	7.339(4)	0.613(23)	11.92(13)	0.0416(18)	0.4406(17)	0.6807(87)	1.163(12)

Table 5. Volume (V in nm^3), LJ and total energies (E_{LJ} and E_{tot} in kJ/mol), diffusion constant (D in 10^{-5} cm^2/sec), shear viscosity (η in mp), and thermal conductivities (λ in 10^{-4} cal/Kemsec) of mixtures of argon and krypton at state B (T = 135 K and p = 39.5 atm) as a function of krypton mole fraction, x. Uncertainties in the last reported digit(s) are given in parenthesis

x	V	$-E_{LJ}$	$-E_{tot}$	D	η	λ_{dm}	λ_{pm}	λ_{tr}	λ_{tot}
0	106.2(8)	4.118(7)	2.434(7)	8.254(63)	1.456(12)	0.3336(32)	0.5857(87)	0.4729(50)	1.392(17)
1/6	103.3(6)	4.697(9)	3.013(9)	6.404(66)	1.838(5)	0.2713(38)	0.6092(93)	0.4926(37)	1.373(16)
1/3	101.9(7)	5.256(9)	3.573(9)	5.151(79)	2.202(19)	0.2251(45)	0.6178(80)	0.5002(77)	1.343(19)
1/2	101.5(9)	5.796(7)	4.112(7)	4.202(66)	2.604(14)	0.1896(26)	0.6140(60)	0.5106(29)	1.314(12)
2/3	101.6(7)	6.335(4)	4.651(4)	3.471(30)	3.072(14)	0.1569(17)	0.6082(68)	0.5190(52)	1.284(14)
5/6	102.3(7)	6.851(4)	5.167(4)	2.827(57)	3.640(30)	0.1298(18)	0.5774(96)	0.5304(81)	1.238(20)
1	103.2(8)	7.371(9)	5.687(9)	2.220(29)	4.472(40)	0.1078(15)	0.5480(63)	0.5503(32)	1.206(11)

and (7)) in NpT ensembles obtained from our EMD simulations are listed in Table 4 for stat A (T = 94.4 K and p = 1 atm) and in Table 5 for state B (T = 135 K and p = 39.5 atm), respectively. The calculated diffusion coefficient and shear viscosity for pure liquids at both states are close to the experimental measures (D = 2.43 × 10^{-5} cm^2/sec at 90 K and 1.374 g/cm^3 for pure Ar,[34] η = 1.97 mp at state A for pure Ar,[35] 0.740 mp at state B for pure Ar,[36] and 3.016 mp at state B for pure Kr[36]). The viscosities for pure liquids at state B obtained by non-equilibrium molecular dynamics (NEMD) simulations using the same LJ and the highly accurate Barker-Fisher-Watts (BFW) potentials are superior to our EMD results (0.885 mp and 0.780 mp for the LJ and BFW potentails, respectively, for pure Ar, and 3.425 mp and 3.146 mp for pure Kr).[37]

The composition dependencies of the diffusion coefficient (D), shear viscosity (η), and D*η are also shown in Figure 6 for state A and Figure 7 for state B. The linear model for ideal liquid mixtures, Eq. (16), for each property is shown in the figures as a solid line. Clearly, the diffusion coefficient

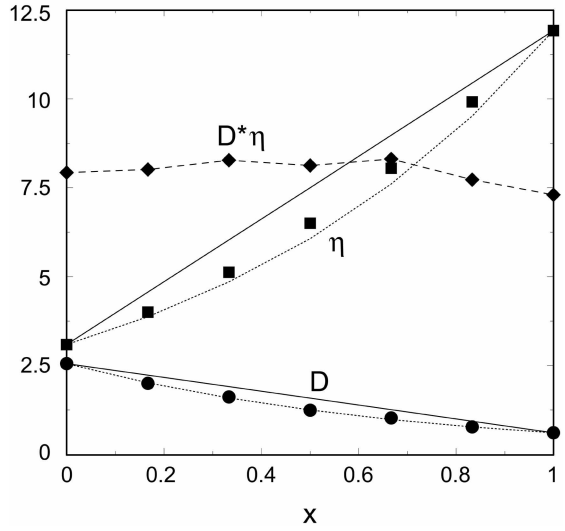

Figure 6. Diffusion constant (D in 10^{-5} cm^2/sec), shear viscosity (η in mp), and D*η as a function of krypton mole fraction, x, at state A (94.4 K and 1 atm) in NpT ensemble.

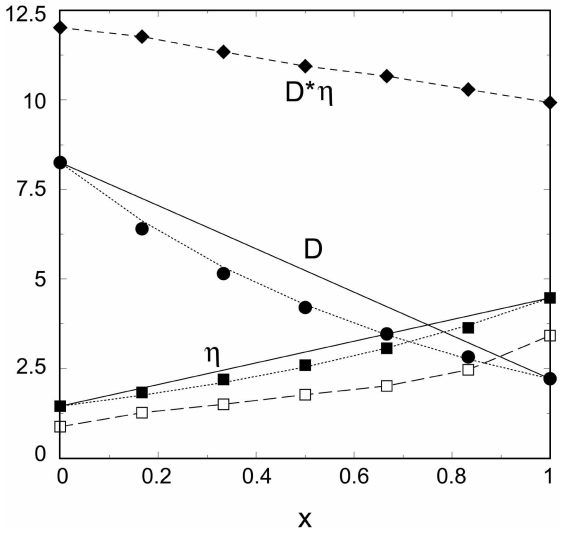

Figure 7. Diffusion constant (D in 10^{-5} cm^2/sec), shear viscosity (η in mp), and D*η as a function of krypton mole fraction, x, at state B (135 K and 39.5 atm) in NpT ensemble. □: the viscosities obtained by non-equilibrium molecular dynamics (NEMD) simulations[37] using the same LJ potentials at state B.

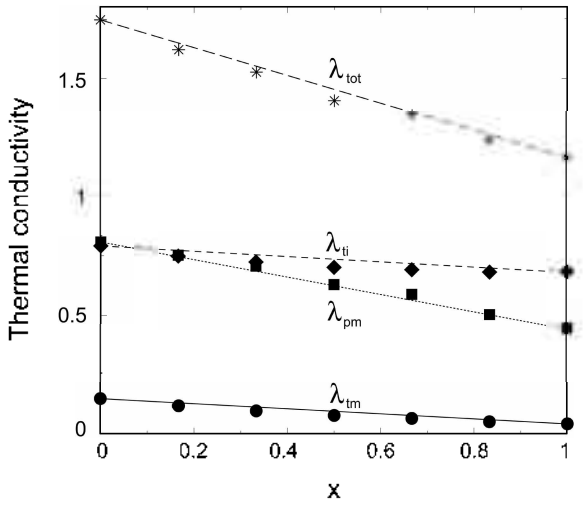

Figure 8. Thermal conductivities (λ in 10^{-4} cal/K·cm·sec) as a function of krypton mole fraction, x, at state A (94.4 K and 1 atm) in NpT ensemble.

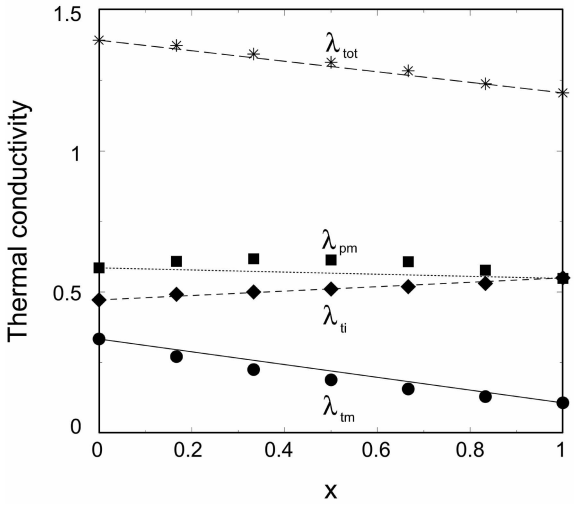

Figure 9. Thermal conductivities (λ in 10^{-4} cal/Kcmsec) as a function of krypton mole fraction, x, at state B (135 K and 39.5 atm) in NpT ensemble.

and shear viscosity at both states differs noticeably from the linear model. In Figures 6 and 7, an exponential model, given by

$$Y = \exp[(1-x)\ln Y_{Ar} + x \ln Y_{Kr}], \qquad (18)$$

is also shown. This model is an engineering correlation recommended for predicting liquid mixtures in the absence of mixture property data. It is superior to the simple linear model because it is clear that this correlation predicts accurately the diffusion coefficients at both states and the shear viscosity at state B except that it underpredicts the shear viscosity at state A. The product $D^*\eta$ is expected to be constant at all the Kr mole fractions, and it is almost constant at state A, while it decreases with increasing x at state B. In Figure 7, the viscosities obtained by non-equilibrium molecular dynamics (NEMD) simulations[37] using the same LJ potentials at state B are compared with our EMD results. The NEMD results are superior to our EMD results when compared experimental viscosities at x = 0 and x = 1 (0.740 mp and 3.016 mp, respectively).

Thermal conductivities for pure liquids and Ar-Kr mixtures through the Green-Kubo formula (Eq. (8)) in NpT ensembles obtained from our EMD simulations are listed in Table 4 for stat A (T = 94.4 K and p = 1 atm) and in Table 5 for state B (T = 135 K and p = 39.5 atm), respectively. The only available experimental thermal conductivity is 2.74 × 10^{-4} cal/Kcmsec at state A for pure Ar,[35] which is close to that from our EMD result. Switching from state A to state B causes to decrease the total thermal conductivity for pure Ar but to increase it for pure Kr. Note that switching from state A to state B causes to increase the diffusion conductivity and to decrease the shear viscosity for both pure liquids.

The composition dependencies of the thermal conductivities are also shown in Figure 8 for state A and Figure 9 for state B. The straight lines for each property in Figures 8 and 9 represent the linear model for ideal liquid mixtures, Eq. (16), and each property hardly deviates from the linear model behaviour. Clearly, the total thermal conductivities at both states A and B obtained from our EMD simulations decrease with the increase of the Kr mole fraction x.

Generally speaking, energy transported *via* molecular motion governs heat conduction in gases, while energy transfer between molecules due to molecular interaction is a dominant factor in heat conduction in liquids. Liquid molecules transport energy by molecular motion and transfer their energy to other molecules by molecular interaction. Accordingly, λ_{tm} and λ_{pm} are the thermal conductivities by the translational and the potential energy transport, respectively, due to molecular motion, and λ_{ti} is that by the translational energy transfer due to molecular interaction. In Figure 8, all three components of thermal conductivity at state A and hence the total thermal conductivity decrease

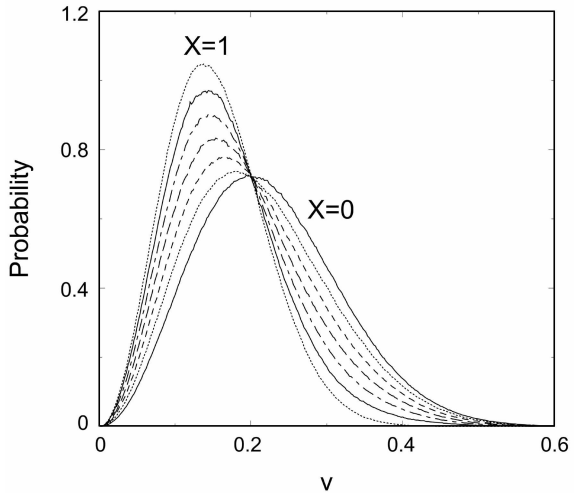

Figure 10. Speed distribution for Ar-Kr mixtures as a function of krypton mole fraction, x, at state A (94.4 K and 1 atm) in NpT ensemble.

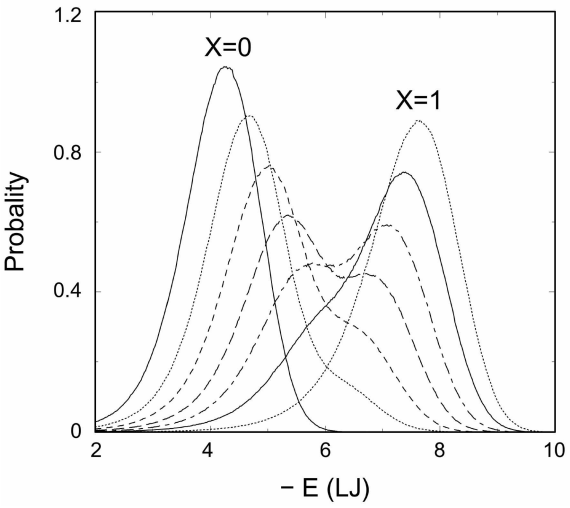

Figure 11. Potential energy distribution for Ar-Kr mixtures as a function of krypton mole fraction, x, at state B (135 K and 39.5 atm) in NpT ensemble.

with the increase of the Kr mole fraction x. The change in λ_{pm} is dominant over those in λ_{pm} and λ_{ti}. At state B, in Figure 9, λ_{tm} decreases, λ_{ti} increases, and λ_{pm} increases and decreases with x. The change in λ_{tm} is dominant over those in λ_{pm} and λ_{ti}, and hence the total thermal conductivity decrease with the increase of the Kr mole fraction x. At both states λ_{pm} or λ_{tm} overrules λ_{ti} in contrast with the general trend in heat conduction in liquid.

In Figure 10, we plot speed distribution for Ar-Kr mixtures as a function of krypton mole fraction, x, at state A in NpT ensemble. The speed distribution shifts to lower speed as the Kr mole fraction x increases due to the heavier Kr mass. The heat flux by molecular motion of translational energy, Eq. (12), and hence the thermal conductivities by the translational energy transport due to molecular motion, λ_{tm}, decrease with the increase of the Kr mole fraction x as shown in Figures 8 and 9.

In Figure 11, we also plot the Lennard-Jones potential energy distribution for Ar-Kr mixtures as a function of krypton mole fraction, x, at state B in NpT ensemble. The energy distribution shifts to higher energy as the Kr mole fraction x increases. The heat flux by molecular motion of potential energy, Eq. (13), has two opposite components - speed and energy, in which the former decreases and the latter increases with increasing x. The thermal conductivities by the potential energy transport due to molecular motion, λ_{pm}, decreases with increasing x as shown in Figure 8, but increases and decreases with increasing x in Figure 9.

The translational heat flux by molecular interaction, Eq. (14), involved with two terms - velocity and interatomic force, which are not easily analyzed. It may be only deduced that the interatomic forces are more contributed to λ_{ti} in smaller volume change in state B than in state A with increasing x from that the thermal conductivities by the translation energy transfer due to molecular interaction, λ_{ti}, decreases with increasing x as shown in Figure 8 (state A), but increases with increasing x in Figure 9 (state B).

Conclusion

We presents new results for transport properties of argon-krypton mixtures at two liquid states (94.4 K and 1 atm; 135 K and 39.5 atm) by equilibrium molecular dynamics (EMD) simulations using modified Green-Kubo formulas. Volume at state A as a function of the Kr mole fraction, x, is close to the linear model for ideal liquid mixtures, while that at state B differs noticeably from the linear model probably due to the high pressure. On the other hand, the energies at both states show a perfect linear model.

In the radial distribution functions for pure liquids at both states, the positions and the heights of the first peaks reflect the magnitude of the LJ parameters σ and ε, respectively. Switching from state A to state B causes to decrease the heights of the first peaks keeping the positions of the first peaks same. In the radial distribution functions for the Ar-Kr mixture (x = 2/3) at state A, he first peak of g_{11} is higher than that of g(r) for pure Ar and the first peak of g_{22} is lower than that of g(r) for pure Kr. The is a mixing effect.

The diffusion coefficient and shear viscosity at both states differs noticeably from the linear model for ideal liquid mixtures. An exponential model of engineering correlation is superior to the simple linear model because it is clear that this correlation predicts accurately the diffusion coefficients at both states and the shear viscosity at state B except that it underpredicts the shear viscosity at state A. Thermal conductivity consists of three contributions by the translational (λ_{tm}) and the potential energy transport (λ_{pm}), respectively, due to molecular motion, and by the translational energy transfer due to molecular interaction (λ_{ti}). All three components of thermal conductivity at state A and hence the total thermal conductivity decrease with the increase of x. At state B, λ_{tm} decreases, λ_{ti} increases, and λ_{pm} increases and decreases with x. The change in λ_{tm} is dominant over those in λ_{pm} and λ_{ti}, and hence the total thermal conductivity decrease with the increase of x.

Acknowledgment. This research was supported by Kyungsung University Research Grants in 2007.

References

1. Rotenberg, A. *J. Chem. Phys.* **1965**, *43*, 4377.
2. Singer, J. V. L.; Singer, K. *Molec. Phys.* **1972**, *24*, 357.
3. McDonald, I. R. *Molec. Phys.* **1972**, *23*, 41.
4. Gardner, P. J.; Heyes, D. M.; Preston, S. R. *Molec. Phys.* **1991**, *73*, 141.
5. Vogelsang, R.; Hoheisel, C.; Paolini, G. V.; Cicotti, G. *Phys. Rev. A* **1987**, *36*, 3964.
6. Hafskjol, B.; Ikeshoji, T.; Ratkje, S. K. *Molec. Phys.* **1993**, *80*, 1389.
7. Ryckaert, J.-P.; Bellemans, A.; Cicotti, G.; Paolini, G. V. *Phys. Rev. A* **1989**, *39*, 259.
8. Heyes, D. M. *Phys. Rev. B* **1988**, *37*, 5677.
9. Borgelt, P.; Hoheisel, C.; Stell, G. *Phys. Rev. A* **1990**, *42*, 789.
10. Evans, D. J. *Phys. Rev. A* **1981**, *23*, 1988.
11. Evans, D. J. *Phys. Rev. A* **1986**, *34*, 1449.
12. Cummings, P. T.; Varner, T. L. *J. Chem. Phys.* **1988**, *89*, 6391.
13. MacGowan, D.; Evans, D. J. *Phys. Rev. A* **1986**, *34*, 2133.

14. Evans, D. J.; MacGowan, D. *Phys. Rev. A* **1987**, *36*, 948: Paolini, G. V.; Ciccotti, G. *Phys. Rev. A* **1987**, *35*, 5156.
15. MacGowan, D. *Phys. Rev. A* **1987**, *36*, 1367.
16. Nakanishi, K.; Narusawa, H.; Toukubo, K. *J. Chem. Phys.* **1980**, *72*, 3089.
17. Hoheisel, C.; Vogelsang, R. *Comput. Phys. Rep.* **1988**, *8*, 1.
18. Vogelsang, R.; Hoheisel, C. *J. Chem. Phys.* **1988**, *89*, 1588.
19. MacGowan, D. *Molec. Phys.* **1986**, *59*, 1017.
20. Jolly, D. L.; Bearman, R. J. *Molec. Phys.* **1980**, *41*, 137.
21. Toxvaerd, S. *Molec. Phys.* **1985**, *56*, 1017.
22. Bearman, R. J.; Jolly, D. L. *Molec. Phys.* **1981**, *44*, 665.
23. Bearman, R. J.; Jolly, D. L. *Molec. Phys.* **1984**, *51*, 447.
24. Evans, D. J.; Hanley, H. J. M. *Phys. Rev. A* **1979**, *20*, 1648.
25. Hanley, H. J. M.; Evans, D. J. *Molec. Phys.* **1980**, *39*, 1039.
26. Murad, S.; Sethi, D. P. S.; Ravi, P. V. *Fluid Phase Equilib.* **1989**, *53*, 159: Murad, S. *A.I.Ch.E. J.* **1989**, *35*, 311.
27. Street, W. B.; Staveley, L. A. K. *J. Chem. Phys.* **1967**, *47*, 2449.
28. Gauss, K. F. *J. Reine Angew. Math.* **1829**, *IV*, 232.
29. Hoover, W. G.; Evans, D. J.; Hickman, R. B.; Ladd, A. J. C.; Ashurst, W. T.; Moran, B. *Phys. Rev. A* **1980**, *22*, 1690.
30. Allen, M. P.; Tildesley, D. J. *Computer Simulation of Liquids*; Oxford Univ. Press: Oxford, 1987; p 64.
31. Allen, M. P.; Tildesley, D. J. *Computer Simulation of Liquids*; Oxford Univ. Press: Oxford, 1987; p 81.
32. Gear, C. W. *Numerical Initial Value Problems in Ordinary Differential Equations*; Englewood Cliffs: NJ, Prentice Hall, 1971.
33. Lee, S. H. *Bull. Kor. Chem. Soc.* **2007**, *28*, 1317.
34. Naghizadeh, J.; Rice, S. A. *J. Chem. Phys.* **1962**, *36*, 2710.
35. Cook, G. A. *Argon, Helium and the Rare Gases*; Interscience: NY, 1961. Obtained from Lagrange interpolation of experimental results at 94.4 K.
36. Rabinovich, V. A.; Vasserman, A. A.; Nedostup, V. I.; Veksler, L. S. *Thermodynamic Properties of Neon, Argon, Krypton and Xenon*; Hemisphere: Washington D. C., 1988.
37. Lee, S. H.; Cummings, P. T. *J. Chem. Phys.* **1993**, *99*, 3919.